Am J Physiol Heart Circ Physiol 309: H1964–H1973, 2015.
First published September 25, 2015; doi:10.1152/ajpheart.00055.2015.

Role of atrial tissue remodeling on rotor dynamics: an in vitro study

Andreu M. Climent,[1] María S Guillem,[2] Lucia Fuentes,[1] Peter Lee,[3,4] Christian Bollensdorff,[5] María Eugenia Fernández-Santos,[1] Susana Suárez-Sancho,[1] Ricardo Sanz-Ruiz,[1] Pedro Luis Sánchez,[1] Felipe Atienza,[1] and Francisco Fernández-Avilés[1]

[1]*Cardiology Department, Hospital General Universitario Gregorio Marañón, Instituto de Investigación Sanitaria Gregorio Marañón, Madrid, Spain;* [2]*ITACA Institute, Universitat Politécnica de Valencia, Valencia, Spain;* [3]*Essel Research and Development, Toronto, Canada;* [4]*Division of Cardiology, Toronto General Hospital, Toronto, Canada; and* [5]*Sidra Medical and Research Center, Division of Cardiovascular Research, Doha, Qatar*

Submitted 22 January 2015; accepted in final form 18 September 2015

Climent AM, Guillem MS, Fuentes L, Lee P, Bollensdorff C, Fernández-Santos ME, Suárez-Sancho S, Sanz-Ruiz R, Sánchez PL, Atienza F, Fernández-Avilés F. Role of atrial tissue remodeling on rotor dynamics: an in vitro study. *Am J Physiol Heart Circ Physiol* 309: H1964–H1973, 2015. First published September 25, 2015; doi:10.1152/ajpheart.00055.2015.—The objective of this article is to present an in vitro model of atrial cardiac tissue that could serve to study the mechanisms of remodeling related to atrial fibrillation (AF). We analyze the modification on gene expression and modifications on rotor dynamics following tissue remodeling. Atrial murine cells (HL-1 myocytes) were maintained in culture after the spontaneous initiation of AF and analyzed at two time points: 3.1 ± 1.3 and 9.7 ± 0.5 days after AF initiation. The degree of electrophysiological remodeling (i.e., relative gene expression of key ion channels) and structural inhomogeneity was compared between early and late cell culture times both in nonfibrillating and fibrillating cell cultures. In addition, the electrophysiological characteristics of in vitro fibrillation [e.g., density of phase singularities (PS/cm^2), dominant frequency, and rotor meandering] analyzed by means of optical mapping were compared with the degree of electrophysiological remodeling. Fibrillating cell cultures showed a differential ion channel gene expression associated with atrial tissue remodeling (i.e., decreased SCN5A, CACN1C, KCND3, and GJA1 and increased KCNJ2) not present in nonfibrillating cell cultures. Also, fibrillatory complexity was increased in late- vs. early stage cultures (1.12 ± 0.14 vs. 0.43 ± 0.19 PS/cm^2, $P < 0.01$), which was associated with changes in the electrical reentrant patterns (i.e., decrease in rotor tip meandering and increase in wavefront curvature). HL-1 cells can reproduce AF features such as electrophysiological remodeling and an increased complexity of the electrophysiological behavior associated with the fibrillation time that resembles those occurring in patients with chronic AF.

atrial fibrillation; optical mapping

NEW & NOTEWORTHY

This is the first report to detect electrophysiological remodeling related with an increased fibrillation complexity in in vitro atrial cell cultures. Our results show that prolonged in vitro fibrillation produced variations of genetic expression (SCN5A, CACN1C, KCND3, GJA1, and KCNJ2) and fibrillation reentrant wavefronts that resemble those observed in human atrial fibrillation.

ATRIAL FIBRILLATION (AF) requires a triggering mechanism and a cardiac substrate that allows the perpetuation of the reentrant activity (14). Studies have shown that, in paroxysmal AF, the arrhythmia is hierarchically maintained by a limited number of regions preferentially located at the pulmonary veins that can be eliminated by means of targeted radiofrequency ablation (3, 4, 12). However, in chronic AF patients more extensive ablation strategies are needed to restore sinus rhythm. It is believed that this is a consequence of tissue remodeling in the atrium (8). Specifically, remodeling refers to changes in atrial tissue structural and electrophysiological properties following periods of sustained AF (35).

The evaluation of antiarrhythmic treatments that can mitigate or reverse the effects of remodeling and restore sinus rhythm in chronic AF requires the development of experimental models that reproduce key features of electrical and/or structural remodeling. However, the development of effective research models of chronic AF is one of the main barriers to elucidating the underlying mechanisms of this arrhythmia and enabling design of effective therapies. Atrial murine immortalized cells (HL-1) under conditions of fast activation rates display some characteristics consistent with fibrillation-related remodeling as those found in atrial tissue from patients with chronic AF (7, 30, 31).

Building on the previous studies, we have analyzed the relation between HL-1 cell culture remodeling due to in vitro fibrillation and the different degrees of electrophysiological complexity. In the present study, we analyzed the mechanisms of rotor dynamics that promote increased fibrillation complexity and related them to electrophysiological remodeling and structural inhomogeneities arising from sustained in vitro arrhythmia. Finally, we tested the hypothesis that a reduction in the rotor core excitability would increase meandering and promote arrhythmia termination due to collisions, either between rotors or with anatomical obstacles.

METHODS

Experimental protocol. HL-1 cells were maintained, grown, and proliferated according to the protocol established by Claycomb et al. (9) in 6-cm-diameter petri dishes. Under these culture conditions, cells spontaneously presented fibrillatory activity after a mean of 53 ± 17 h, as detected by measuring the activation rate in bright-field microscopy videos. During spontaneous nonfibrillatory activation, HL-1 cells showed a slow activation rate of 1.4 ± 0.5 beats/s. After achieving further cell confluency, HL-1 cells sustained faster fibrillatory rates of 3.1 ± 0.2 Hz. To evaluate the time-dependent effects of fibrillation on AF complexity, cell cultures were divided into two groups based on the incubation period following the initiation of AF: *1*) early: 3.1 ± 1.3 days ($N = 10$) and *2*) late: 9.7 ± 0.5 days ($N = 8$). For each group, optical mapping recordings (4 s duration) were acquired under basal conditions and after the administration of verapamil (4 μM in Krebs solution). In addition to calcium imaging, *1*)

Address for reprint requests and other correspondence: A. M. Climent: Laboratory of Bioartificial Organs. Dept. of Cardiology. Instituto de Investigación Sanitaria Gregorio Marañón. Hospital General Universitario Gregorio Marañón. Edificio Materno Infantil. C\ O'Donnell 48, 28009, Madrid, España (e-mail: acliment@cardiovascularcelltherapy.com).

structural homogeneity was assessed analyzing bright-field microscopy images from several regions across the dish and *2*) electrophysiological remodeling was evaluated by the RT-PCR process. To analyze the differential influence of the fibrillatory activity and duration between early and late-stage groups, their genetic expression was compared with nonfibrillating control groups (a nonfibrillating early stage and a nonfibrillating late-stage group). Specifically, HL-1 cells were cultured under the same conditions but in ad hoc petri dishes of 3×3 mm. These small dimensions did not allow HL-1 cell cultures to maintain reentries and fibrillation processes. The mean activation rate of these control cell culture groups was 1.25 ± 0.2 for the early stage and 1.42 ± 0.2 for the late stage (P = not significant).

Finally, to ensure that cell culture over long periods of time does not produce dramatic changes on cell culture conditions, levels of apoptosis were analyzed in both early and late-stage groups by cell labeling with annexin V conjugated with fluorescein isothiocyante (FITC), which recognizes phosphatidylserine exposure on the outer leaflet of the plasma membrane, and with propidium iodide for cell integrity recognition (apoptosis detection kit; Pharmingen). Automatic detection of cytometry quadrants was based on the identification of annexin V-propidium iodide (PI)-negative (i.e., healthy cells) and annexin V-PI-positive populations (i.e., noninteger cells) independently of the basal level of fluorescence of the FITC.

Calcium dye loading. For calcium transient (CaT) imaging, HL-1 cell cultures were stained by immersion in Claycomb culture medium with rhod 2-AM (Ca^{2+}-sensitive probe; TEFLabs, Austin, TX) dissolved in DMSO (1 mM stock solution; 3.3 μl/ml in culture medium) and probenecid (TEFLabs) at 420 μM for 30 min under incubation conditions. After dye incubation, culture medium was changed to fresh modified Krebs solution at 36.5°C [containing (in mM): 120 NaCl, 25 $NaHCO_3$, 1.8 $CaCl_2$, 5.4 KCl, 1 $MgCl_2$, 5.5 glucose, and 1.2 $H_2O_4PNa{\cdot}H_2O$]. All chemicals were obtained from Sigma-Aldrich (Dorset, UK) or Fisher Scientific.

Optical mapping. To excite rhod 2, cell cultures were illuminated with a filtered green light emitting diode (LED) light source: LED CBT-90-G (peak power output 58 W; peak wavelength 524 nm; Luminus Devices), with a plano-convex lens (LA1951; focal length = 25.4 mm; Thorlabs) and a green excitation filter (D540/25X; Chroma Technology). Two such light sources were used to achieve homogeneous illumination. Fluorescence was recorded with an electron-multiplying charge-coupled device (Evolve-128: 128×128, 24×24-μm square pixels, 16 bit; Photometrics, Tucson, AZ), with a custom emission filter (ET585/50–800/200M; Chroma Technology) suitable for rhod 2 emission placed in front of a high-speed camera lens (DO-2595; Navitar).

Calcium image processing. Custom software written in MATLAB was used to perform optical mapping image processing. Specifically, the organization of fibrillatory activity was estimated as the mean number of simultaneous functional reentrant activities. Those reentries were automatically identified as singularity points that remained stable over time and space by applying phase map analysis. Phase maps of each movie were obtained by calculating the instantaneous phase of the Hilbert-transformed optical recordings (35). The phase signal ranges between 0 and 2π represent the relative delay of each signal in one period. A singularity point was defined as the point in a phase map that is surrounded by phases from 0 to 2π. These phase transitions were evaluated at three concentric circles centered at each evaluated point. Phase singularities (PS) were defined as points at which the phases in at least two of these three circles were required to fulfill the following two conditions: *1*) phase transition between two consecutive pixels not exceeding 0.6π and *2*) monotonic phase changes. Once all singularity points were identified, they were connected in time and space into rotors. Unstable rotors with durations of <100 ms were discarded. The complexity of the fibrillatory activity was defined as the mean number of simultaneous functional reentries per square centimeter. In addition, the meandering of each individual rotor was defined as the distance covered by the tip divided by the duration of the PS (i.e., cm/s). Rotor meandering in each cell culture was calculated as the mean value of the meandering of all the PS detected during the recording.

To estimate rotor curvature, lines connecting phase transitions from 0 to 2π that originate at each rotor were selected. These transition lines were traced from the rotor tip to the periphery, and the relative angle (α) and distance (δ) of line points with respect to the rotor tip were computed. The curvature at each point in the transitional line was measured as the spatial derivative of α ($d\alpha/d\delta$). Finally, the curvature of the rotor was estimated as the mean value of curvature along the transitional line.

Power spectra of optical signals were estimated by using a Welch periodogram (2-s Hamming window overlap). Dominant frequency (DF) of each pixel was determined as the frequency with the largest peak in the spectrum between 0.05 and 30 Hz. For each individual cell culture, the highest DF was defined as the maximum DF of the entire dish.

Gene expression analysis. Total RNA from HL-1 cell cultures of all four groups were isolated using Tri-reagent (Sigma). Transcripts were quantified in a two-step RT-PCR. First-strand cDNA was synthesized using the High Capacity cDNA Reverse Transcription Kit (Applied Biosystems) with random hexamers. Next, samples were run using SYBR Green oligonucleotides and the CFX Real Time PCR detection systems (Bio-Rad). The analysis was customized, with three biological replicates per target gene, and two technical replicates for each sample. Gene expression values were normalized to two standard housekeeping genes (36b4 and cyclophylin) as internal controls, and expressed as relative mRNA levels (relative expression). Data were automatically analyzed using the CFX gene expression analysis software (Bio-Rad). Primer sequences are summarized in Table 1. Specifically, variation in the expression of genes (SCN5A, CACNA1C, KCND3, KCNJ2, KCNH2, GJA5, GJA1, and GJA7) involved in the ion currents voltage-activated sodium channel current (I_{Na}), L-type calcium channel current (I_{CaL}), the transient outward potassium channel current (I_{to}), inward-rectifier potassium current (I_{K1}), rapid potassium ion current (I_{Kr}), connexin (Cx) 40, Cx43, and Cx45 were compared between early and late stage of both fibrillating and nonfibrillating cell groups.

Immunohistochemistry and microscopy. To quantify the degree of structural heterogeneities produced during long incubation times, the

Table 1. *Primers used for RT-PCR*

Gene	Protein	Forward Primer (5′-3′)	Reverse Primer (5′-3′)
SCN5A	Nav1.5	CACCTTCACCGCCATCTACA	AAGGTGCGTAAGGCTGAGAC
CACNA1C	Cav 1.2	CCTCGAAGCTGGGAGAACAG	TGTGTGGGAGTCAATGGAGC
KCND3	Kv 4.3	TGCCTAAGACAATCGCAGGG	TGTGCAGGTAGGCATTGGAG
KCNJ2	Kir 2.1	GACGCCTTCATCATTGGTGC	CCGGACATGAGCTTCCACAA
KCNH2	Kv11.1	ATGGCTCAGATCCAGGCAGTTA	CAAGGAGAGCGGTCAGGTAATG
GJA5	Con 40	ATACCATTCAGCCTGGTTGC	GGTGGGCCTCTTTAGCTTTC
GJA1	Con 43	GGACTGCTTCCTCTCACGTC	CAGCTTGTACCCAGGAGGAG
GJA7	Con 45	TTTGTGTGCAACACAGAGCA	GGTCCTCTTCCGTTTCTTCC
36B4		GCGACCTGGAAGTCCAACTA	ATCTGCTGCATCTGCTTGG
CYCLOPHYLIN		ACAGGTCCTGGCATCTTGTC	CATGGCTTCCACAATGTTCA

inhomogeneity of cell cultures was quantified based on the gray level co-occurrence matrix of bright-field images (13). In short, texture is quantified by constructing a probability matrix of the co-ocurrence of pairs of gray tones in a given direction and in which the number of gray levels is limited to *N*. In particular, we converted our images into eight gray tones and measured co-ocurrence in the horizontal direction only. The gray level co-ocurrence matrix, therefore, is defined as described in *Eq. 1*:

$$\mathbf{C}(m,n) = \sum_x \sum_y P\{\mathbf{I}(x,y) = m \,\&\, \mathbf{I}(x+1,y) = n\} \qquad (1)$$

where (x,y) are the horizontal and vertical coordinates of the analyzed pixel, P is the probability of co-ocurrence where $P[\bullet] = 1$ if the argument is true and $P[\bullet] = 0$ otherwise, $\mathbf{I}$ is the image matrix, and m and n are gray levels from 0 to 7.

Inhomogeneity of an image (ψ), therefore, can be computed from matrix $\mathbf{C}$ as described in Eq. 2:

$$\psi = 1 - \frac{\sum_{m,n} \frac{\mathbf{C}(m,n)}{1 + |m-n|}}{N_{xy}} \qquad (2)$$

where N_{xy} is the number of pixels in the image.

This indirect measurement was validated by correlating cell culture inhomogeneity with the number of cell nuclei measured in a subset of cell cultures labeled with 4′,6-diamidino-2-phenylindole (DAPI, D8417, 1 mg/ml stock solution in ultrapure water; Sigma-Aldrich). Specifically, the correlation between the number of nuclei measured in DAPI images and the inhomogeneity measurement was 0.98 ($P < 0.01$).

Statistical analysis. Data are presented as means ± SD. Cross correlation was used to estimate the relationship between the number of nuclei in DAPI images and the homogeneity of the bright-field images. Continuous baseline variables were compared using Student's *t*-test or Mann-Whitney test, depending on the variable's statistical distribution. Accuracy of linear regression curves was expressed as the coefficient of determination (R^2).

RESULTS

In vitro AF. In Fig. 1*A* a representative phase map of an in vitro AF episode is shown. In this example, a counterclockwise rotor can be seen in the top right area of the dish (*point 1*), whereas several wavebreaks and secondary rotors can be seen in the rest of the dish. After the DF map was analyzed, a frequency gradient from the top right corner to the lower portion of the dish could be observed (Fig. 1*B*). In Fig. 1*C*, the time-space plot of the vertical line across the rotor tip in the phase map shows that activity around the main rotor is peri-

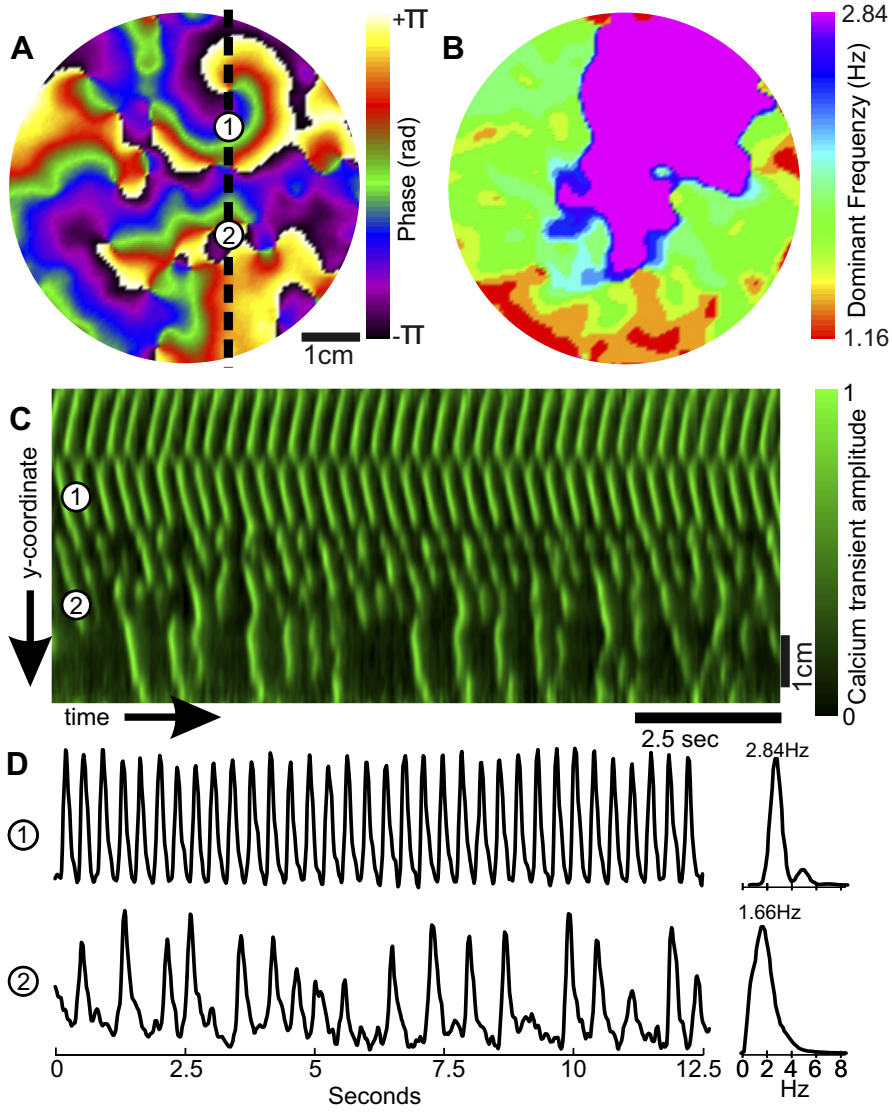

Fig. 1. Illustrative example of in vitro early stage atrial fibrillation. *A*: phase map of calcium transients showing a fast stable rotor at the *top right* area of the dish. *B*: dominant frequency map demonstrating a frequency gradient from the *top right* to the *bottom* region of the dish. *C*: time-space plot of activity across the line defined by *points 1* and *2*, as shown in *A*. *D*: time series of calcium transient optical signals (*left*) and their corresponding power spectrum (*right*), from *points 1* and *2*.

odical over time while calcium waves distal from the rotor present an irregular pattern (fragmentation of the propagating wavefronts). The inhomogeneous propagation of wavefronts originating from the stable rotor produced an irregular activation pattern characteristic of AF. Figure 1*D* shows the time evolution of CaT from two camera pixels and their corresponding power spectra. It can be seen that the activation rate of cells distal from the rotor are slower than that of cells around the rotor (i.e., 1.66 vs. 2.84 Hz). The spectral concentration of the frequency components was higher for cells at *point 1* than those at *point 2*, consistent with the decreased activation regularity of cells distal from the rotor.

Relationship between atrial tissue remodeling and fibrillation complexity. We observed that the duration of fibrillation significantly modified the complexity of the electrophysiological propagation patterns of HL-1 cells. The number of singularity points per square centimeter at baseline was significantly higher in the late- than in the early stage group (i.e., 1.12 ± 0.14 vs. 0.43 ± 0.19 PS/cm^2, $P < 0.01$). In Fig. 2*A*, normalized CaT and phase map images of a representative cell culture from each group are shown. In the early stage example (Fig. 2*A*, *left*), a single rotor located in the upper left region of the dish generated relatively regular wavefronts that covered most of the dish (see Supplemental Video 1). However, at the periphery of the dish, small wavebreaks produced a significant number of singularity points. In contrast, several small wavefronts and phase singularities were observed without a clear predominant rotor in late-stage cultures (see Supplemental Video 2).

The rotation period of each rotor was measured, and the correlation between the fastest rotor and the inverse of the highest DF was computed for both groups (Fig. 2*B*). A significant correlation was found between both parameters (i.e., $R^2 = 0.98$, $P < 0.01$), demonstrating that rotors were responsible for the highest activation rates maintaining fibrillation in both early and late-stage cell cultures.

The relationship between the structural complexity of HL-1 cell cultures and their electrophysiological behavior was evaluated by analyzing the degree of cellular inhomogeneity from bright-field microscopy images. In Fig. 2*C*, bright-field and immunohistochemistry (i.e., DAPI) microscopy images of two representative examples of fibrillating HL-1 cell cultures with different degrees of complexity are shown. In the fibrillating Hl-1 cell group, longer time cultures were associated with a higher inhomogeneity of bright-field images (i.e., 29.56 ± 1.6% of inhomogeneity in the early stage group vs. 33.56 ± 0.6% in the late-stage group, $P < 0.01$). In the nonfibrillating HL-1 cell group, the differences in the degree of inhomogeneity between early and late-stage groups were significantly lower than in the fibrillating group (i.e., 4 ± 1% in the fibrillating group vs. 2 ± 0.4% in the nonfibrillating group, $P < 0.05$). This result suggests that the observed structural remodeling in the fibrillating group was a combination of both proliferation of cells and remodeling due to fibrillation. In the fibrillating group, the number of singularity points per square centimeter showed a direct correlation with the degree of inhomogeneity in the corresponding bright-field microscopy images ($R^2 = 0.78$, $P < 0.01$).

The increase in the complexity of long-term cultures in the fibrillating group was associated with an electrical remodeling of HL-1 cells as assessed measuring ionic channel gene expressions (Fig. 3). RT-PCR analysis showed a significant reduction in the expression of genes SCN5A, CACNA1C, KCND3, and GJA1, which codify for proteins involved in the regulation of I_{Na}, I_{CaL}, I_{to}, and Cx43, respectively. In contrast, there was a significant increase in the gene expression of the I_{K1} (i.e., KCNJ2). Interestingly, in the nonfibrillating group these alterations on SCN5A, CACNA1C, or GJA1 were not detected, and the variations of KCND3 and KCNJ2 were in the opposite direction as those of the fibrillating group. Regarding

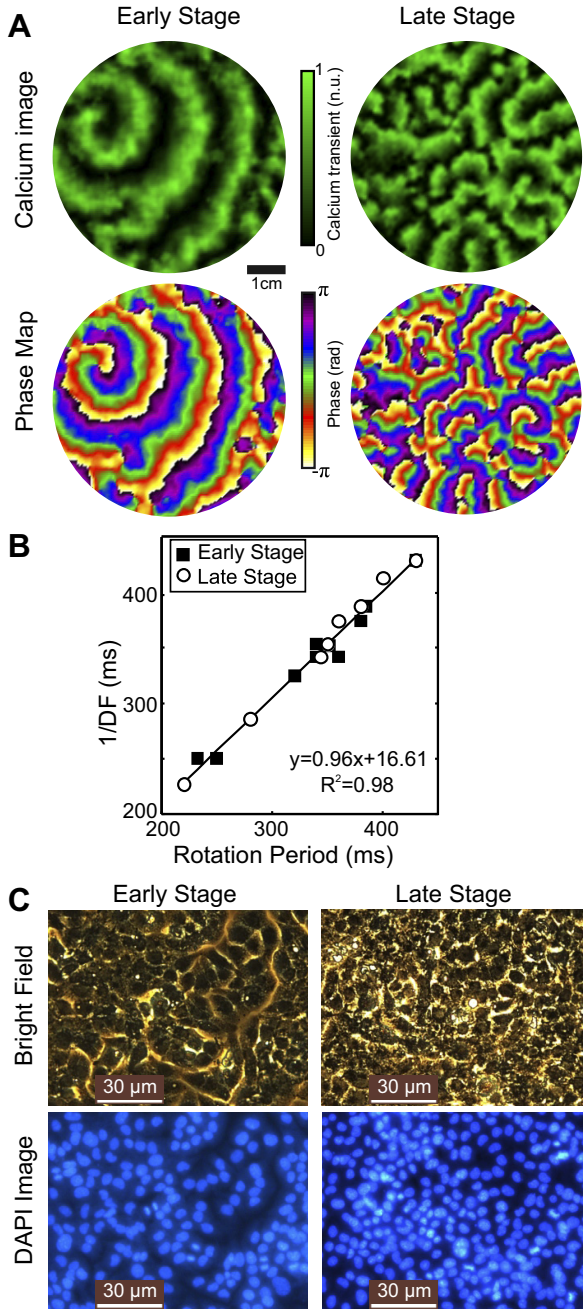

Fig. 2. Comparison between early and late-stage fibrillating cell cultures. *A*: calcium transient (CaT) and phase maps of representative cell cultures from each group. *B*: correlation between the shortest rotation period and dominant cycle length [1/dominant frequency (DF)]. *C*: representative examples of bright-field and 4′,6-diamidino-2-phenylindole (DAPI) images for the early and late-stage cell cultures.

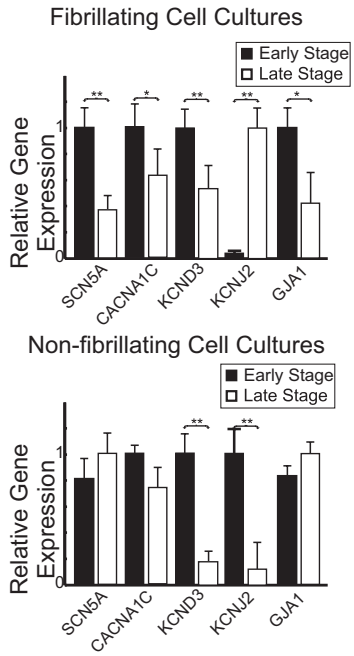

Fig. 3. Expression of genes SNC5A, CACNA1C, KCND3, KCNJ2, and GJA1 in early and late-stage groups of both fibrillating and nonfibrillating cell cultures. These genes codify for proteins that are molecular components of ion channels associated with voltage-activated sodium channel current (I_{Na}), L-type calcium channel current (I_{CaL}), transient outward potassium channel current (I_{to}), inward-rectifier potassium current (I_{K1}), and Cx43 current, respectively. *$P < 0.05$ and **$P < 0.01$.

the other genes analyzed (i.e., KCNH2, GJA5, and GJA7, which are involved in the codification of I_{Kr}, Cx40, and Cx45, respectively), no significant differences were found between early and late stages of the fibrillating and the nonfibrillating group.

Regarding the effects of culture times with cell metabolism, results of annexin-V FITC/PI analysis for the fibrillating group are depicted in Fig. 4. Notice that longer culture times did not imply an increase in the number of apoptotic cells, although the number of detritus in the media was significantly higher. However, no significant differences were found between the fibrillation and a nonfibrillating group, indicating that gene expression variations shown in Fig. 3 may not be dependent on the metabolic variations due to longer culturing periods.

Rotor dynamics and fibrillation complexity. To evaluate the electrophysiological mechanisms responsible for increased fibrillation complexity in the late-stage group, DF, mean conduction velocity (CV), rotor curvature, and rotor meandering (mean distance traveled for each rotor over time) were measured and compared between groups.

As observed in Fig. 5*A*, there was no clear correlation between the DF and electrical activity complexity. Furthermore, no significant differences in DFs were found between early and late-stage groups (i.e., 3.02 ± 0.56 vs. 2.83 ± 1.43 Hz). According to our results, mechanisms that could explain the increased complexity in the late-stage group could be: *1*) a reduction in the CV and/or *2*) a modification in the rotor dynamics. Although late-stage cultures presented a significantly lower CV than the early stage group (i.e., 2.0 ± 0.6 vs. 3.2 ± 1.0 cm/s, $P < 0.01$) that could be explained either by a higher cell density or by the reduction in the expression of Cx43 and/or I_{Na} (Fig. 3), CV had a weak correlation with complexity (i.e., $R^2 = 0.44$, Fig. 5*B*). In contrast, rotor dynamics (i.e., wavefront curvature and rotor meandering) were significantly correlated with electrical complexity ($R^2 = 0.86$ and 0.79, respectively, Fig. 5, *C* and *D*).

Analysis of verapamil-induced changes in in vitro AF. To further confirm that fibrillation complexity was mainly governed by rotor dynamics and to test the hypothesis that rotor instability could facilitate the termination of AF, fibrillation activity was analyzed 5 min following verapamil administration. Verapamil is known to increase the size of the rotor meandering area by means of the reduction of the rotor core excitability (27). Figure 6 shows phase maps, DF maps, and

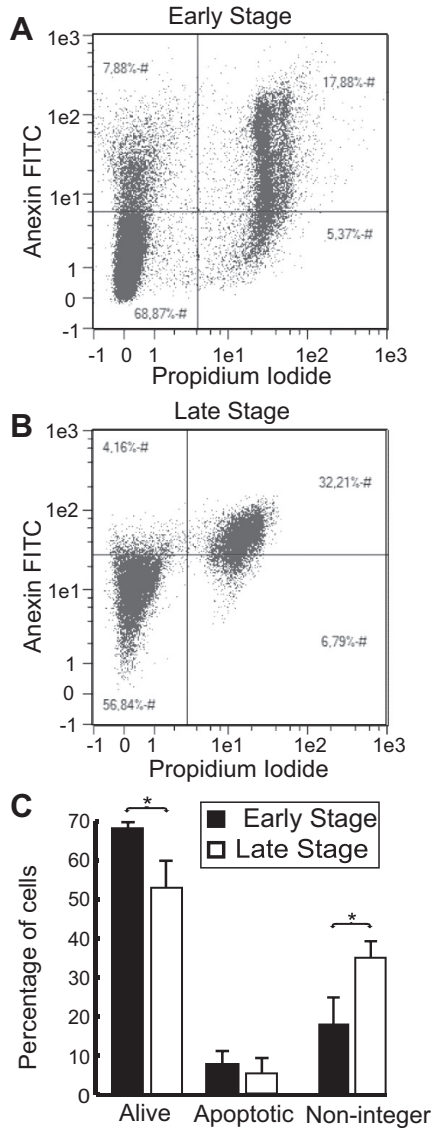

Fig. 4. Annexin V conjugated with fluorescein isothiocyanate (FITC) flow cytometry assay. *A* and *B*: representative examples of the fibrillating early and late-stage groups; the four quadrants were automatically adjusted in each experiment independent of the basal-nonspecific FITC fluorescence by detecting healthy [i.e., annexin V^-/propidium iodide $(PI)^-$ populations] and noninteger (i.e., annexin V^+/PI^+ populations) cell populations. *C*: summary of assay results for the fibrillating groups, including healthy cells, apoptotic cells, and detected cells without full cell integrity. The results are represented as means ± SE of 8 independent experiments. *$P < 0.05$.

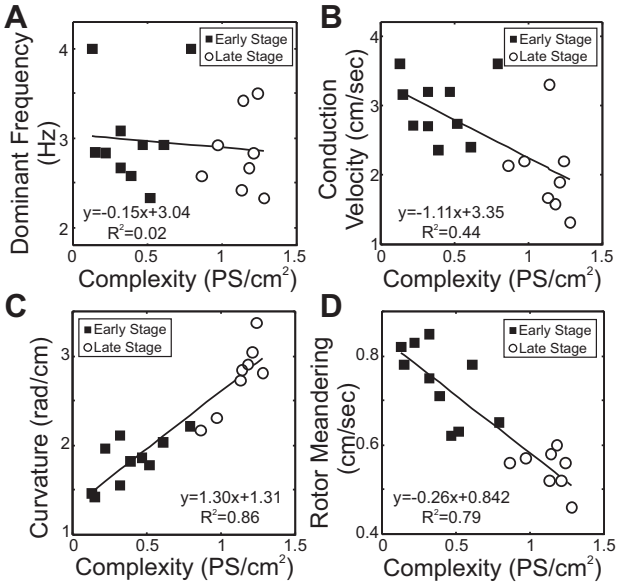

Fig. 5. Correlation between the electrophysiological complexity, measured as the no. of phase singularities per square centimeter, and the highest dominant frequency (*A*), mean conduction velocity (*B*), rotor curvature (*C*), and rotor meandering (*D*).

CaTs at baseline and following verapamil administration for a representative example from each group. As shown in the phase map snapshots, the number of simultaneous rotors and their curvature were significantly reduced following verapamil administration. This reduction in fibrillatory complexity led to a decrease in the activation rate, as shown in the DF maps and representative CaT signals (Fig. 6).

Figure 7*A* shows the effect of verapamil on fibrillation complexity in both cell culture groups. Not only was there a reduction in complexity, but infusion of verapamil resulted in arrhythmia termination after 10 min in five cell cultures from the early stage group. In addition, for the late-stage group, fibrillation complexity following verapamil administration was reduced to values similar to basal conditions of the early stage group (Fig. 7*A*). This reduction in the complexity was not associated with significant modifications of the CV (Fig. 7*B*). However, administration of verapamil resulted in a nonuniform decrease of the DF (Fig. 7*C*); the late-stage culture group had higher dominant frequencies after drug infusion compared with the early stage group. With regard to the rotor dynamics, the average meandering of each rotor significantly increased in both early and late-stage groups (Fig. 7*D*). This increase in the rotor tip movement was associated with a reduction in the rotor curvature in both groups (Fig. 7*E*). Those modifications in rotor dynamics increased the area needed for each rotor to be self-sustained and could explain the reduction in the complexity.

DISCUSSION

Major findings. The main finding of the present study is that atrial HL-1 cell cultures can reproduce in vitro AF with different degrees of electrophysiological complexity and tissue remodeling resembling processes that occur in AF patients during the transition from paroxysmal to persistent AF. To our knowledge, this is the first study in which the duration of culture has been shown to be correlated with both cell remodeling and the degree of electrophysiological complexity of fibrillation. In addition, our results suggest that rotor dynamics (i.e., meandering and wavefront curvature) play an important role in the formation of complex patterns and could be considered as useful surrogates for the efficacy of novel antiarrhythmic therapies.

Research models of chronic AF. Atrial tissue remodeling occurs during the transition from paroxysmal to chronic AF, giving rise to more complex fibrillation activity of persistent AF patients (2). Atrial remodeling appears as a consequence of multiple factors, such as ion channel expressions and higher degrees of fibrosis that ultimately result in dilation of the atria and a reduction of atrial contractility (1).

These differences in the electrophysiological mechanisms that govern paroxysmal and chronic AF may explain the observed divergences in the outcome and response to treatment between these two groups of patients (4, 8). A critical obstacle for the elucidation of mechanisms responsible for chronic AF lies in the practical challenges associated with the development of experimental models that reproduce the electrophysiological characteristics of atrial remodeling. Animal models involve subjecting animals to weeks or months of sustained atrial arrhythmias, which implies significant economical, ethical, and time burdens (11, 20). Other experimental models include in vitro cell cultures, which are typically obtained from neonatal rat hearts. Because neonatal cells do not reproduce the electrophysiological complexity of remodeled tissue, they have been cocultured with myofibroblasts (35). However, a major drawback is that this model predominantly displays a nonadult ventricular phenotype. In contrast, the HL-1 cell line (9) is the only available cell line that reproduces the features of adult atrial cardiomyocytes (33). In addition, HL-1 cells under fast activation rates present structural and electrophysiological changes such as reduced plasmalemmal levels of L-type Ca^{2+} α_{1C}-subunit, myolysis, nuclear condensation, and an increase in calpain activity (7), characteristic of remodeled myocytes. Our results are consistent with these experiments and further indicate that HL-1 cells maintained under spontaneously induced fibrillation present a reduction in I_{Na}, I_{CaL}, I_{to}, and Cx43 ion channel gene expressions and an increase in I_{K1} gene expression, whereas nonfibrillating long-term HL-1 cell cultures did not present this gene expression remodeling, and, therefore, these changes can be attributed to fibrillation-induced remodeling and not culture time. This electrical remodeling is similar to what has been observed in the sheep atrial cardiomyocytes (20) and in patients with long-term AF (10). However, the analysis of other currents that may play an important role in AF remodeling (e.g., Cx40, Cx45, and I_{Kr}) did not show significant variations between early and late stages neither in the fibrillating group nor in the nonfibrillating group.

Mechanisms for an increased complexity in remodeled AF. In the present study we aimed to elucidate the mechanisms that produce an increase in fibrillation complexity in HL-1 cells during long periods of sustained fibrillation. Because the so called funny current is present in HL-1 cells, they can develop spontaneous action potentials. Thus, it could be hypothesized that the increase in the complexity of late-stage cultures is related to an increased probability of spontaneous cell activation, resulting in more wavebreaks. However, this study dem-

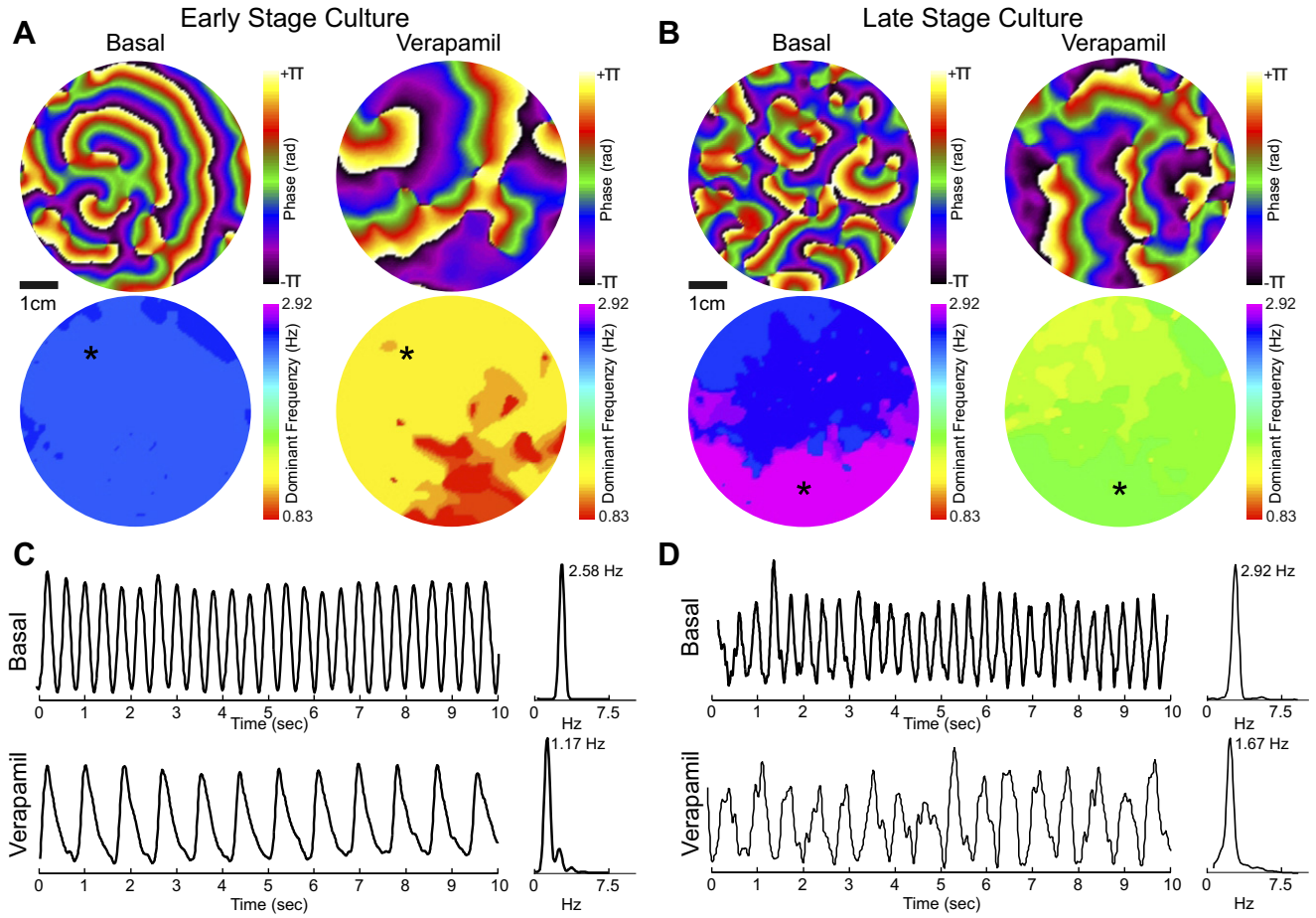

Fig. 6. Effects of verapamil on activation maps and the frequency domain. Snapshots of phase maps (*top*) and dominant frequency maps (*bottom*) during basal conditions (*left*) and after administration of verapamil (*right*) in an illustrative case for early (*A*) and late (*B*)-stage groups. Time series of calcium transient optical signals (*left*) and the corresponding power spectrum (*right*) of the starred region during basal conditions (*top*) and after the administration of verapamil (*bottom*) for the early stage (*C*) and late-stage (*D*) groups.

onstrates that functional reentry, and not spontaneous activations or calcium releases, is the underlying mechanism of the sustained fibrillation in both early and late-stage HL-1 cell cultures.

The increase in fibrillation complexity in the late-stage group was associated with a reduction in tip meandering and an increase of reentrant wavefront curvature, allowing the formation of more simultaneous rotors. These phenomena are usually associated with shorter action potentials and refractory periods (25), which is consistent with the observed reduction of the I_{CaL} and the increase in I_{K1}. In fact, both computer simulations (15, 24) and experimental studies (28) demonstrated that an unpregulation of I_{K1} is associated with a reduction in rotor tip meandering and a decrease in the area required to maintain the reentry (24). An additional contribution to fibrillation complexity in our late-stage cultures may be an increased cellular heterogeneity in this group. Although the mechanisms of our in vitro model may be different, an increased heterogeneity has been found in persistent AF patients mainly because of atrial tissue fibrosis, which has shown to promote irregular reentry formation (21, 35).

Persistent AF is usually characterized by higher DFs than paroxysmal AF, both in animals and patients (2, 20). These higher DFs have been associated with a reduction in the time required by a rotor to complete a period due to *1*) the reduction of the area of reentry (i.e., rotor meandering) and *2*) an increase of the CV as a consequence of a higher sodium channel availability consequence of the cell hyperpolarization linked with the I_{K1} upregulation (25). Our results demonstrate that the late-stage group presented a reduction in the rotor meandering and an increase in I_{K1} expression that was associated with a higher complexity. However, we did not observe a faster activation rate most likely because of a reduction in the CV because of a higher cell density in the late-stage group and/or a reduction in the expression of I_{Na} channels and Cx43. These results agree with recent studies that showed a significant reduction in Cx43 due to AF both in pigs (5) and humans (18), in which this reduction was also associated with an increased complexity of the electrophysiological activity.

Interestingly, the administration of verapamil, an L-type calcium channel blocker, resulted in a reduction of fibrillation complexity and a reduction in the DF. This reduction in the DF may seem paradoxical since verapamil shortens the effective refractory period that, in principle, should allow for faster activation rates (23, 26). However, this DF reduction can be explained by the modification in the rotor dynamics induced by verapamil; both in the early and late-stage groups the blockade of the late calcium current by verapamil increased the area

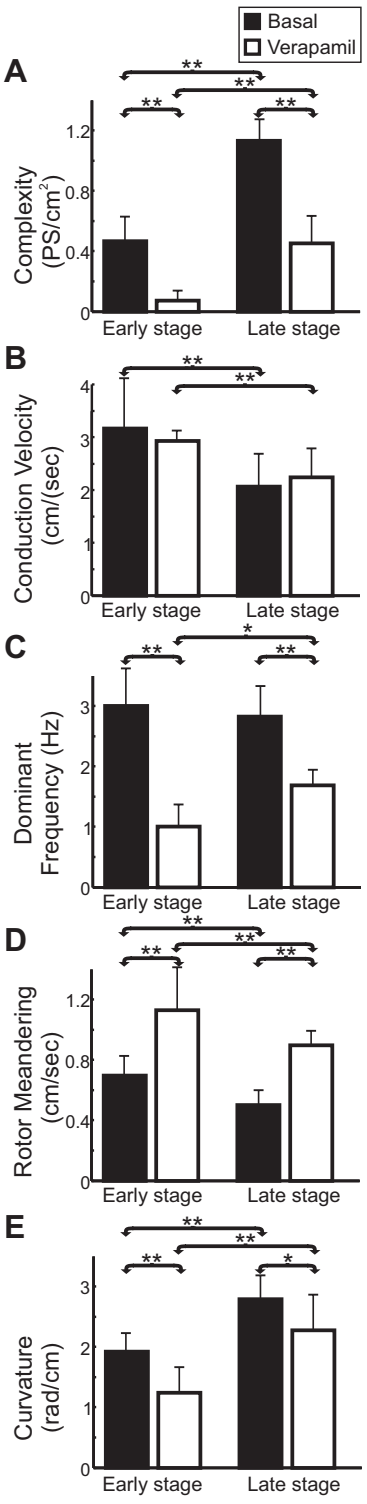

Fig. 7. Quantification of verapamil effects on the electrophysiological characteristics of both early and late-stage culture groups. *A*: complexity measured as the no. of simultaneous phase singularities per square centimeter. *B*: conduction velocity. *C*: dominant frequency. *D*: rotor meandering (mean distance traveled for each rotor over time). *E*: mean curvature of rotors. $*P < 0.05$ and $**P < 0.01$.

needed for each individual rotor to complete a rotation. The enlargement of the distance that a rotor needs to travel to complete a rotation implies a rotation period lengthening in the absence of CV modifications, and thus a reduction in the DF. This reduction was not uniform in both groups, since, after the administration of verapamil, DF of the late-stage group was significantly higher than for the early stage group. Concomitantly, a wider rotor tip meandering implies an increment in the probability of collision between rotors. This increased probability of collisions, together with a decrease in the rotor curvature in both groups (Fig. 7*E*), resulted in a widening of the area required by a rotor to be self-sustained. As a consequence, the number of rotors per area unit was reduced and even terminated in the early stage group. This effect of verapamil on fibrillation complexity is consistent with previous observations in isolated hearts (27) and clinical patients (6) and confirms the important role of calcium homeostasis in the mechanisms of AF.

In summary, the results of the present study are in agreement with the contention that rotors play the key role in AF maintenance since the degree of fibrillation complexity depends on reentry curvature and meandering but not necessarily on tissue refractoriness (25). However, the specific mechanisms by which calcium channel blockers increase rotor meandering remain unclear. Further studies are needed to clarify the role of calcium currents in reentrant dynamics and more specifically the relation between calcium channel dynamics and rotor meandering.

Limitations. The present study was performed using immortalized murine atrial cells, which are currently the only myocardial cell line with a relatively mature phenotype. However, in vitro studies are only partial representations of in vivo scenarios, and HL-1 cell cultures and human atrial tissue present electrophysiological differences evidenced in our results (e.g., continuous proliferation, lower CV and DFs during fibrillation), and, for this reason, extrapolation of these results to human AF should be performed with care.

In the clinical setting, remodeling of atrial tissue takes weeks, months, or even years. Here we evaluated differences that occurred in a time interval of a week. These electrophysiological alterations were observable due to the rapid maturation process of HL-1 cells, which may be influenced by their continuous proliferation. The observed remodeling in the fibrillating group could be superimposed to the ongoing process of remodeling that these cells may suffer due to culture for long periods of time (e.g., increase of number of cells, development of a disorganized 3-dimensional structure, and/or metabolically deprived regions, etc.). However, no remodeling in the genetic expression in the nonfibrillating group and no differences in apoptosis levels were found between the fibrillating and nonfibrillating groups. In fact, HL-1 cells have shown to retain a cardiac phenotype even for culture periods of 30 days or more (29). These results suggest that, despite the fact that specific mechanisms involved in HL-1 cell remodeling may differ significantly from those that take place in human chronic AF (7, 30), the described in vitro remodeling is a first, although important, step in the study of AF remodeling mechanisms. For example, the recent development of human cardiac myocytes derived from pluripotent stem cells (16, 17) may allow the use of in vitro models of human AF in the near future and should serve to extend our study to a more clinically relevant setting.

In conclusion, HL-1 cells can reproduce AF features such as frequency gradients and mother rotors, giving rise to a hierarchical fibrillatory pattern similar to that described in sheep (19)

and human (3, 22) AF. In addition, our results demonstrate that the remodeling process of HL-1 cell cultures occurs after several days in culture and resembles that occurring in patients with chronic AF. Modifications in rotor dynamics may underlie the increased complexity of remodeled cell cultures and arise as potential targets for arrhythmia termination. Therefore, this model could be useful for studying the effect of remodeling on fibrillation mechanisms and the development of more effective treatments.

GRANTS

This work was supported in part by grants from the Spanish Ministry of Science and Innovation (PLE2009-0152), the Instituto de Salud Carlos III (Ministry of Economy and Competitiveness, Spain: PI13-01882, PI13-00903, and TEC2013-50391-EXP), and the Red de Investigación Cardiovascular (RIC) from Instituto de Salud Carlos III (Ministry of Economy and Competitiveness, Spain).

DISCLOSURES

Dr. Felipe Atienza served on the advisory board of Medtronic and has received research funding from St. Jude Medical Spain. None of the companies disclosed financed the research described in this manuscript.

AUTHOR CONTRIBUTIONS

Author contributions: A.M.C., M.S.G., F.A., and F.F.-A. conception and design of research; A.M.C., L.F., P.L., C.B., M.E.F.-S., and S.S.-S. performed experiments; A.M.C., M.S.G., L.F., and S.S.-S. analyzed data; A.M.C., M.S.G., L.F., P.L., C.B., S.S.-S., R.S.-R., P.L.S., F.A., and F.F.-A. interpreted results of experiments; A.M.C. and M.S.G. prepared figures; A.M.C. and M.S.G. drafted manuscript; A.M.C., M.S.G., L.F., P.L., C.B., M.E.F.-S., S.S.-S., R.S.-R., P.L.S., F.A., and F.F.-A. edited and revised manuscript; A.M.C., M.S.G., L.F., P.L., C.B., M.E.F.-S., S.S.-S., R.S.-R., P.L.S., F.A., and F.F.-A. approved final version of manuscript.

REFERENCES

1. **Allessie M, Ausma J, Schotten U.** Electrical, contractile and structural remodeling during atrial fibrillation. *Cardiovasc Res* 54: 230–246, 2002.
2. **Allessie MA, de Groot NM, Houben RP, Schotten U, Boersma E, Smeets JL, Crijns HJ.** Electropathological substrate of long-standing persistent atrial fibrillation in patients with structural heart disease: longitudinal dissociation. *Circ Arrhythm Electrophysiol* 3: 606–615, 2010.
3. **Atienza F, Almendral J, Jalife J, Zlochiver S, Ploutz-Snyder R, Torrecilla EG, Arenal A, Kalifa J, Fernández-Avilés F, Berenfeld O.** Real-time dominant frequency mapping and ablation of dominant frequency sites in atrial fibrillation with left-to-right frequency gradients predicts long-term maintenance of sinus rhythm. *Heart Rhythm* 6: 33–40, 2009.
4. **Atienza F, Almendral J, Ormaetxe JM, Moya A, Martínez-Alday JD, Hernández-Madrid A, Castellanos E, Arribas F, Arias MÁ, Tercedor L, Peinado R, Arcocha MF, Ortiz M, Martínez-Alzamora N, Arenal A, Fernández-Avilés F, Jalife J, Investigators RADARAF.** Comparison of Radiofrequency Catheter Ablation of Drivers and Circumferential Pulmonary Vein Isolation in Atrial Fibrillation: A Noninferiority Randomized Multicenter RADAR-AF Trial. *J Am Coll Cardiol* 64: 2455–2467, 2014.
5. **Bikou O, Thomas D, Trappe K, Lugenbiel P, Kelemen K, Koch M, Soucek R, Voss F, Becker R, Katus HA, Bauer A.** Connexin 43 gene therapy prevents persistent atrial fibrillation in a porcine model. *Cardiovasc Res* 92: 218–225, 2011.
6. **Bollmann A, Sonne K, Esperer HD, Toepffer I, Klein HU.** Patients with persistent atrial fibrillation taking oral verapamil exhibit a lower atrial frequency on the ECG. *Ann Noninvasive Electrocardiol* 7: 92–97, 2002.
7. **Brundel BJ, Kampinga HH, Henning RH.** Calpain inhibition prevents pacing-induced cellular remodeling in a HL-1 myocyte model for atrial fibrillation. *Cardiovasc Res* 1: 521–528, 2004.
8. **Calkins H, Kuck KH, Cappato R, Brugada J, Camm AJ, Chen SA, Crijns HJ, Damiano RJ Jr, Davies DW, DiMarco J, Edgerton J, Ellenbogen K, Ezekowitz MD, Haines DE, Haissaguerre M, Hindricks G, Iesaka Y, Jackman W, Jalife J, Jais P, Kalman J, Keane D, Kim YH, Kirchhof P, Klein G, Kottkamp H, Kumagai K, Lindsay BD, Mansour M, Marchlinski FE, McCarthy PM, Mont JL, Morady F, Nademanee K, Nakagawa H, Natale A, Nattel S, Packer DL, Pappone C, Prystowsky E, Raviele A, Reddy V, Ruskin JN, Shemin RJ, Tsao HM, Wilber D, Heart Rhythm Society Task Force on Catheter, and Surgical Ablation of Atrial Fibrillation.** HRS/EHRA/ECAS expert consensus statement on catheter and surgical ablation of atrial fibrillation: Recommendations for patient selection, procedural techniques, patient management and follow-up, definitions, endpoints, and research trial design. *Heart Rhythm* 9: 632–696, 2012.
9. **Claycomb WC, Lanson NA Jr, Stallworth BS, Egeland DB, Delcarpio JB, Bahinski A, Izzo NJJ.** HL-1 cells: a cardiac muscle cell line that contracts and retains phenotypic characteristics of the adult cardiomyocyte. *Proc Natl Acad Sci USA* 95: 2979–2984, 1998.
10. **Dobrev D, Ravens U.** Remodeling of cardiomyocyte ion channels in human atrial fibrillation. *Basic Res Cardiol* 98: 137–148, 2003.
11. **Filgueiras-Rama D, Price NF, Martins RP, Yamazaki M, Avula UM, Kaur K, Kalifa J, Ennis SR, Hwang E, Devabhaktuni V, Jalife J, Berenfeld O.** Long-term frequency gradients during persistent atrial fibrillation in sheep are associated with stable sources in the left atrium. *Circ Arrhythm Electrophysiol* 5: 1160–1167, 2012.
12. **Haïssaguerre M, Jaïs P, Shah DC, Takahashi A, Hocini M, Quiniou G, Garrigue S, Le Mouroux A, Le Métayer P, Clémenty J.** Spontaneous initiation of atrial fibrillation by ectopic beats originating in the pulmonary veins. *N Engl J Med* 339: 659–666, 1998.
13. **Haralick RM, Shanmugam K, Dinstein I.** Textural features for image classification. *IEEE Trans Sys Man Cybernet* 3: 610–621, 1973.
14. **Jalife J.** Déjà vu in the theories of atrial fibrillation dynamics. *Cardiovasc Res* 89: 766–775, 2011.
15. **Koivumäki JT, Seemann G, Maleckar MM, Tavi P.** In silico screening of the key cellular remodeling targets in chronic atrial fibrillation. *PLoS Comput Biol* 10: e1003620, 2014.
16. **Lee P, Klos M, Bollensdorff C, Hou L, Ewart P, Kamp TJ, Zhang J, Bizy A, Guerrero-Serna G, Kohl P, Jalife J, Herron TJ.** Simultaneous voltage and calcium mapping of genetically purified human induced pluripotent stem cell-derived cardiac myocyte monolayers. *Circ Res* 110: 1556–1563, 2012.
17. **Lieu DK, Fu JD, Chiamvimonvat N, Tung KC, McNerney GP, Huser T, Keller G, Kong CW, Li RA.** Mechanism-based facilitated maturation of human pluripotent stem cell-derived cardiomyocytes. *Circ Arrhythm Electrophysiol* 6: 191–201, 2013.
18. **Liu X, Shi HF, Tan HW, Wang XH, Zhou L, Gu JN.** Decreased connexin 43 and increased fibrosis in atrial regions susceptible to complex fractionated atrial electrograms. *Cardiology* 114: 22–29, 2009.
19. **Mansour M, Mandapati R, Berenfeld O, Chen J, Samie FH, Jalife J.** Left-to-right gradient of atrial frequencies during acute atrial fibrillation in the isolated sheep heart. *Circulation* 103: 2631–2636, 2001.
20. **Martins RP, Kaur K, Hwang E, Ramirez RJ, Willis BC, Filgueiras-Rama D, Ennis SR, Takemoto Y, Ponce-Balbuena D, Zarzoso M, O'Connell RP, Musa H, Guerrero-Serna G, Avula UM, Swartz MF, Bhushal S, Deo M, Pandit SV, Berenfeld O, Jalife J.** Dominant frequency increase rate predicts transition from paroxysmal to long-term persistent atrial fibrillation. *Circulation* 129: 1472–1482, 2014.
21. **McDowell KS, Vadakkumpadan F, Blake R, Blauer J, Plank G, Macleod RS, Trayanova NA.** Mechanistic inquiry into the role of tissue remodeling in fibrotic lesions in human atrial fibrillation. *Biophys J* 104: 2764–2773, 2013.
22. **Narayan SM, Krummen DE, Shivkumar K, Clopton P, Rappel WJ, Miller JM.** Treatment of atrial fibrillation by the ablation of localized sources: CONFIRM (Conventional Ablation for Atrial Fibrillation With or Without Focal Impulse and Rotor Modulation) trial. *J Am Coll Cardiol* 60: 628–636, 2012.
23. **Noguchi K, Masumiya H, Takahashi K, Kaneko K, Higuchi S, Tanaka H, Shigenobu K.** Comparative effects of gallopamil and verapamil on the mechanical and electrophysiological parameters of isolated guinea-pig myocardium. *Can J Physiol Pharmacol* 75: 1316–1321, 1997.
24. **Pandit SV, Berenfeld O, Anumonwo JM, Zaritski RM, Kneller J, Nattel S, Jalife J.** Ionic determinants of functional reentry in a 2-D model of human atrial cells during simulated chronic atrial fibrillation. *Biophys J* 88: 3806–3821, 2005.
25. **Pandit SV, Jalife J.** Rotors and the dynamics of cardiac fibrillation. *Circ Res* 112: 849–862, 2013.
26. **Riccio ML, Koller ML, Gilmour RF Jr.** Electrical restitution and spatiotemporal organization during ventricular fibrillation. *Circ Res* 84: 955–963, 1999.
27. **Samie FH, Mandapati R, Gray RA, Watanabe Y, Zuur C, Beaumont J, Jalife J.** A mechanism of transition from ventricular fibrillation to

tachycardia: effect of calcium channel blockade on the dynamics of rotating waves. *Circ Res* 86: 684–691, 2000.
28. **Samie FH, Berenfeld O, Anumonwo J, Mironov SF, Udassi S, Beaumont J, Taffet S, Pertsov AM, Jalife J.** Rectification of the background potassium current: a determinant of rotor dynamics in ventricular fibrillation. *Circ Res* 89: 1216–1223, 2001.
29. **Smith AW, Segar CE, Nguyen PK, MacEwan MR, Efimov IR, Elbert DL.** Long-term culture of HL-1 cardiomyocytes in modular poly (ethylene glycol) microsphere-based scaffolds crosslinked in the phase-separated state. *Acta Biomater* 8: 31–40, 2012.
30. **Tsai CT, Chiang FT, Chen WP, Hwang JJ, Tseng CD, Wu CK, Yu CC, Wang YC, Lai LP, Lin JL.** Angiotensin II induces complex fractionated electrogram in a cultured atrial myocyte mono-layer mediated by calcium and sodium-calcium exchanger. *Cell Calcium* 49: 1–11, 2011.
31. **Tsai CT, Chiang FT, Tseng CD, Yu CC, Wang YC, Lai LP, Hwang JJ, Lin JL.** Mechanical stretch of atrial myocyte monolayer decreases sarcoplasmic reticulum calcium adenosine triphosphatase expression and increases susceptibility to repolarization alternans. *J Am Coll Cardiol* 58: 2106–2115, 2011.
32. **Tuomi JM, Tyml K, Jones DL.** Atrial tachycardia/fibrillation in the connexin 43 G60S mutant (Oculodentodigital dysplasia) mouse. *Am J Physiol Heart Circ Physiol* 300: H1402–H1411, 2011.
33. **White SM, Constantin PE, Claycomb WC.** Cardiac physiology at the cellular level: use of cultured HL-1 cardiomyocytes for studies of cardiac muscle cell structure and function. *Am J Physiol Heart Circ Physiol* 286: H823–H829, 2004.
34. **Wijffels MC, Kirchhof CJ, Dorland R, Allessie MA.** Atrial fibrillation begets atrial fibrillation. A study in awake chronically instrumented goats. *Circulation* 92: 1954–1968, 1995.
35. **Zlochiver S, Muñoz V, Vikstrom KL, Taffet SM, Berenfeld O, Jalife J.** Electrotonic myofibroblast-to-myocyte coupling increases propensity to reentrant arrhythmias in two-dimensional cardiac monolayers. *Biophys J* 95: 4469–4480, 2008.